Synthesis of Metallo-Polymers and Direct Visualization of Single Polymer Chain

Zhikai Li,[†,‡,⊥] Yiming Li,[‡,⊥] Yiming Zhao,[†,⊥] Heng Wang,[‡] Yuan Zhang,[§,#] Bo Song,[‡] Xiaohong Li,[†] Shuai Lu,[‡,▽] Xin-Qi Hao,[▽] Saw-Wai Hla,[*,§] Yingfeng Tu,[*,†] Xiaopeng Li[*,‡]

[†]Jiangsu Key Laboratory of Advanced Functional Polymer Design and Application, State and Local Joint Engineering Laboratory for Novel Functional Polymeric Materials, College of Chemistry, Chemical Engineering and Materials Science, Soochow University, Suzhou 215123, China

[‡]Department of Chemistry, University of South Florida, Tampa, Florida 33620, United States

[§]Nanoscience and Technology Division, Argonne National Laboratory, Lemont, Illinois 60439, United States

[#]Department of Physics, Old Dominion University, Norfolk, Virginia 23529, United States

[▽]College of Chemistry, Zhengzhou University, Zhengzhou, Henan 450001, China

ABSTRACT: During the past few decades, the study of single polymer chain has attracted considerable attentions with the goal of exploring the structure-property relationship of polymers. It still, however, remains challenging due to the variability and low atomic resolution of amorphous single polymer chain. Here, we demonstrated a new strategy to visualize single metallo-polymer chain with hexameric or trimeric supramolecule as repeat unit, in which Ru(II) with strong coordination and Fe(II) with weak coordination were combined together in a step-wise manner. With the help of ultrahigh-vacuum, low-temperature scanning tunneling microscopy (UHV-LT-STM) and scanning tunneling spectroscopy (STS), we were able to directly visualize both Ru(II) and Fe(II), which act as staining reagents on the repeat units, and thus providing detailed structure information for the single polymer chain. As such, the direct visualization of single random polymer chain is realized to enhance the characterization of polymers at single-molecule level.

Introduction

Over the past decades, in order to enhance the understanding of the structure-property relationship of polymers, characterization of single polymer chain has attracted widespread attentions.[1-2] Microscopy, such as scanning tunneling microscopy (STM) or atomic force microscopy (AFM), allows us to observe the molecular structures directly. However, except for the large biomolecules such as DNA,[3-7] the imaging of structure as well as conformation is mainly limited to crystalline, liquid crystalline, and the aggregation of polymer chains.[8-15] A formidable challenge still remains to address the random coil conformations of amorphous single polymer chain due to the variability and low atomic resolution.

As is known to all, metals or metal ions with high electron density are able to afford relatively strong signals and enhanced atomic resolution under microscopy like STM. Therefore, if one can introduce these metal components into polymer chains as "staining reagents", the amorphous single polymer chain could be easily observed and confirmed by STM depending on the position of metal. Generally, metal components are introduced into polymers through three approaches, *viz.*, 1) polymerization of monomers with metal ions in the main chains or pendant groups;[16-20] 2) supramolecular polymerization through coordination of metal ions with organic monomer in the main chains;[21-31] 3) metalation of pendant groups through post-polymerization modification.[32-43] However, these approaches have certain limitations. In the first approach, the polymerization is typically centered on small and stable metal-organic components, e.g., metallocenes, which are polymerized through living radical polymerization, ring-opening metathesis polymerization (ROMP), etc.[44-46] In the second approach, the supramolecular polymerization is mainly achieved through dynamic coordination interaction.[22, 26-27, 29-31, 47] Therefore, precise control of the polymerization is difficult for dynamic supramolecular polymers with labile coordination bonds. In the third approach, metalation of pendant groups after polymerization is also limited to metal with weak coordination in order to get low-defect polymers.[32, 34-38] To date, very few systems were able to harness both strong and weak coordination metal ions together into metallo-polymers with discrete supramolecules as repeat units.

Thanks to the recent flourish of 2D and 3D metallo-supramolecular structures with precisely-controlled sizes and shapes constructed by coordination-driven self-assembly,[48-72] we introduced two discrete structures, hexameric and trimeric metallo-supramolecules, as repeat units to construct metallo-polymers due to the high symmetry as well as the appropriate size for STM imaging (**Scheme 1**). Copper(I)-catalyzed azide-alkyne cycloaddition (CuAAC) "click" reaction, which owns the advantages of fast reaction rates, and high yields with mild reaction conditions,[73-76] was selected for the polymerization. In this design, we bridged 2,2′:6′,2″-terpyridine (tpy) ligand and Ru(II) with strong coordination interaction to create the open-form metal-organic hexameric and trimeric monomers with free tpy.

Scheme 1. Monomers (A, Hex-M; B, Tri-M and Alkyne-PEG), and Their Corresponding Metallo-Polymers with 2D Hexameric (C) and Trimeric(D) Supramolecules as Repeat Units.

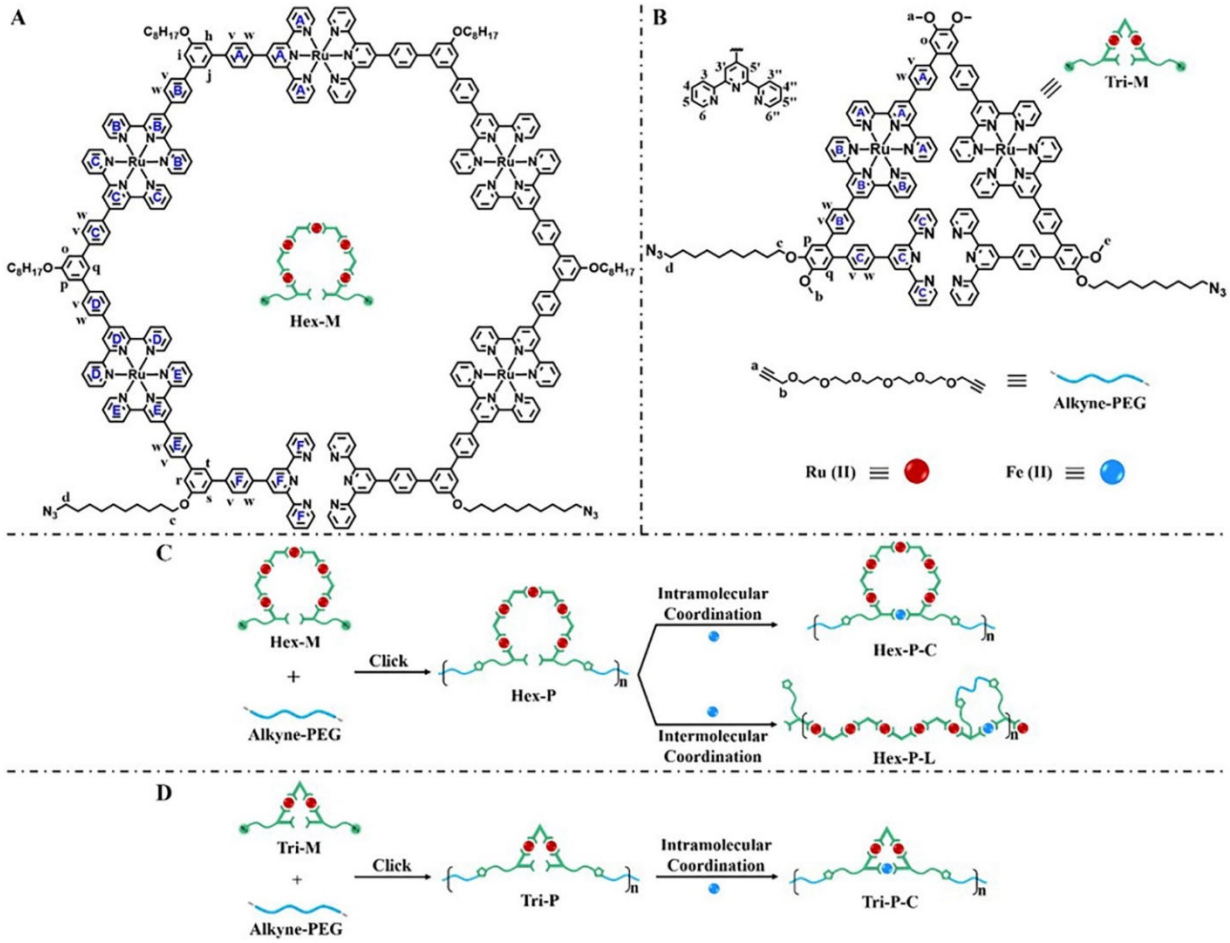

After polymerization by click reaction, through further metalation of Fe(II) with weak coordination, both strong and weak binding metal ions were harnessed into one polymer system in a step-wise manner. Our initial assumption was that the metalation of Fe(II) of metal-organic monomers would form ring-closing hexagon or triangle as repeat units. And we could measure the structure and conformation of the amorphous single polymer chain based on the location of Ru(II) and Fe(II). Unexpectedly, according to the results of ultrahigh-vacuum, low-temperature scanning tunneling microscopy (UHV-LT-STM) and scanning tunneling spectroscopy (STS), both hexagon assembled by intramolecular coordination and linear chains assembled by intermolecular assembly were observed. In contrast, only intramolecular assembly into triangle existed in trimeric repeat units.

Results and Discussion

Scheme 1 depicts the two metal-organic monomers with open-form structures, *viz.*, hexameric monomer (**Hex-M**) and trimeric monomer (**Tri-M**), which were prepared according to the procedure as shown in Supporting Information (**Schemes S1-S5**, **Figures S1-S76**). Briefly, **Hex-M** was synthesized through a well-established step-wise strategy based on the strong connectivity of <tpy-Ru(II)-tpy>,[77-84] by which six ditopic tpy ligands bearing 120-degree angle were bridged linearly with five Ru(II) ions. Similarly, two Ru(II) ions were used to bridge three ditopic tpy ligands with 60-degree angle together to afford **Tri-M**. Note that **Hex-M** and **Tri-M** are functionalized by dual azide groups, which were designed for the next polymerization by click reaction. The ^{1}H NMR spectra of **Hex-M** and **Tri-M** were shown in **Figure 1A** and **1E**, with proton labeling at the top of **Scheme 1**. The assignment of peaks associated with the chemical structure was assisted by the two-dimensional (2D) ^{1}H-^{1}H gCOSY and NOESY NMR spectra (**Figures S41-S44**, and **S71-S74**). After treating the precursors (compounds **8** and **16**) bearing chloride as terminal groups with sodium azide, the triplet peak for methylene unit near chloride at around 3.59 ppm totally disappeared with a new triplet peak at 3.28 ppm appeared, demonstrating that the conversion was completed. The integrals from corresponding peaks fit well with the theoretical value, indicating the high purity of **Hex-M** and **Tri-M**.

The **Hex-M** and **Tri-M** monomers were further characterized by electrospray ionization-mass spectrometry (ESI-MS). **Hex-M** (**Figure 2A**) was observed with a dominant set of peaks with continuous charge states from 6+ to 10+, due to successive loss of the counterions, PF_6^-. The experimental isotope pattern of each charge state agrees well with its theoretical simulation result (Inset and **Figure S46**). The averaged molecular mass is deconvoluted as 7019 Da, which matches the chemical composition $[C_{340}H_{294}N_{42}O_6Ru_5P_{10}F_{60}]$.

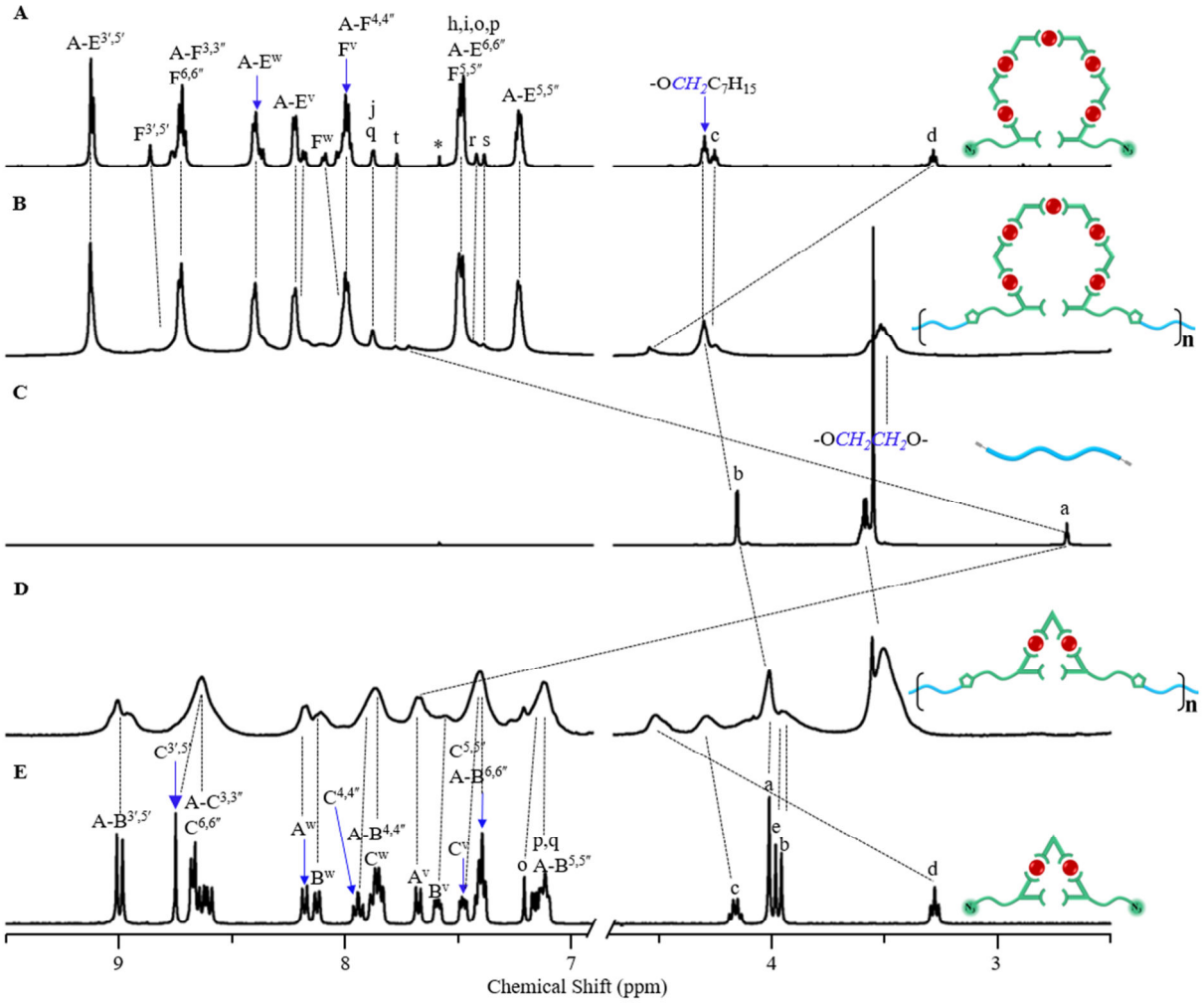

Figure 1. ^{1}H NMR spectra of (A) **Hex-M** (600 MHz), (B) **Hex-P** (600 MHz), (C) **Alkyne-PEG** (400 MHz), (D) **Tri-M** (400 MHz) and (E) **Tri-P** (400 MHz) in CD_3CN. * represents the residue solvent $CHCl_3$.

Figure 2C shows the ESI-MS of **Tri-M** with continuous charge states from 3+ to 4+. The experimental isotope pattern of each charge state is also consistent with the simulated one (Inset and **Figure S76**). The averaged molecular mass is deconvoluted as 3375 Da, which has a good agreement with the chemical composition [$C_{168}H_{142}N_{24}O_6Ru_2P_4F_{24}$]. Furthermore, traveling wave ion mobility-mass spectrometry (TWIM-MS) spectra (**Figure 2B** and **2D**) show a series of narrowly distributed signals with successive charge states for both **Hex-M** and **Tri-M**, indicating high isomeric purity of the structures.

Alkyne-terminated pentaethylene glycol (**Alkyne-PEG, Scheme S6, Figures S77-S79**) was selected as another component to polymerize with the monomers (**Hex-M** and **Tri-M**) to construct the corresponding metallo-polymers (**Hex-P** and **Tri-P**) by click reaction (**Scheme S7**). During the polymerization process in DMF, a large amount of precipitation was produced, suggesting the formation of metallo-polymers (**Hex-P** and **Tri-P**). The products were fully characterized by NMR and matrix-assisted desorption ionization-time of flight (MALDI-TOF). **Figure 1** shows the ^{1}H NMR spectra of **Hex-P** (**Figure 1B**) and **Tri-P** (**Figure 1D**), while 2D ^{1}H-^{1}H gCOSY and NOESY NMR spectra are provided in Supporting Information (**Figures S80-S89**). The triplet peak at 3.28 ppm corresponding to methylene unit near azide group of the monomers (**Hex-M** and **Tri-M**) disappeared, indicating monomers were completely reacted. After the formation of triazole by click reaction, this triplet peak was significantly shifted downfield (~1.23 ppm) and the protons of alkynyl group was dramatically shifted downfield (~4.99 ppm).

MALDI-TOF mass spectrometry provided additional evidence for the formation of metallo-polymer with open-form monomers. In contrast to losing multiple counterions for ESI-MS of monomers, such metallo-polymers are mainly ionized by losing single counterion, that is PF_6^- in this study. **Hex-P** (**Figure 3A**) shows a series of peaks with interval ca. 7340 Da, in a good agreement with the molar mass of the repeat unit in **Hex-P** (**Hex-M** with **Alkyne-PEG**, $C_{356}H_{320}N_{42}O_{12}Ru_5P_{10}F_{60}$; theoretical value: 7334 Da). High molecular weight signal up to 73400 (*m/z*) was detected with the degree of polymerization of 10, directly confirming the successful synthesis of corresponding metallo-polymer **Hex-P**. In terms of polymers with large polydispersity index value (PDI), it is worth noting that MALDI-TOF generally displays a nonsymmetrical distribution of peaks for polymers with higher abundant signals at low *m/z* range due to the high ionization efficiency of spe-

cies with low molecular weight.[85-87] This also suggested that large oligomers with high polymerization degree might exist in our system, however, were not ionized due to the limitation of MALDI-TOF. With small monomer **Tri-M**, much higher degree of polymerization was detected in **Tri-P** as shown in **Figure 3B**. High molecular weight signal up to 70000 (*m/z*) was obtained with the degree of polymerization of 19, indicating the successful synthesis of corresponding metallo-polymer **Tri-P**. The average interval between adjacent peaks is about 3684 Da, which agrees with the molar mass of the repeat unit in **Tri-P** (**Tri-M** with **Alkyne-PEG**, $C_{184}H_{168}N_{24}O_{12}Ru_2P_4F_{24}$; theoretical value: 3689 Da).

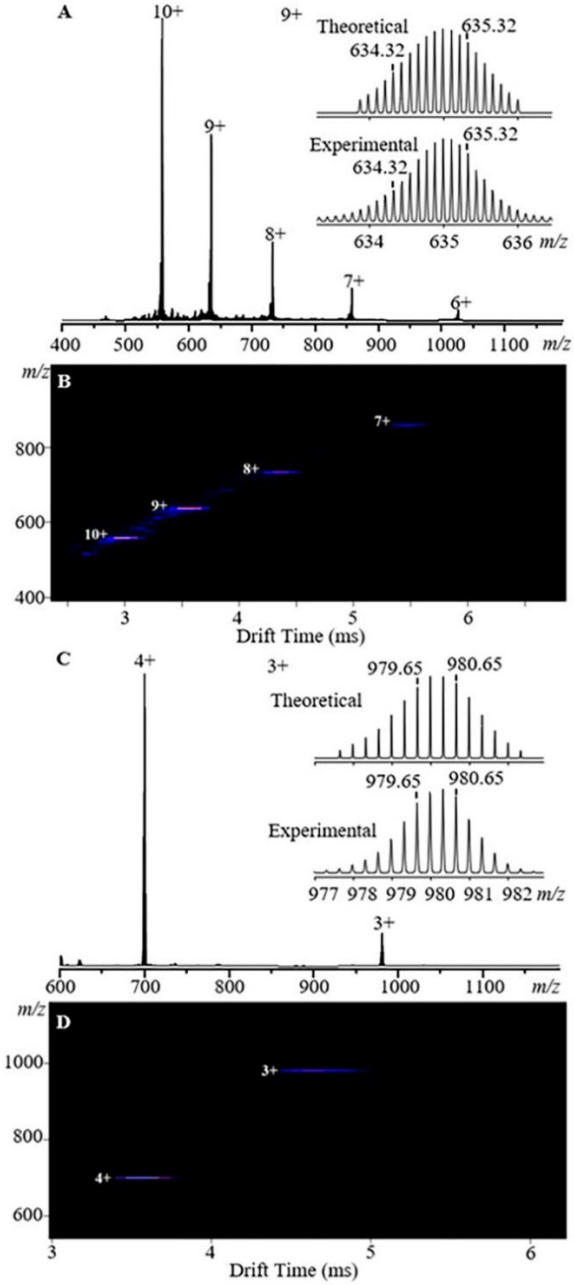

Figure 2. ESI-MS of **Hex-M** (A), TWIM-MS plot (*m/z* vs drift time) of **Hex-M** (B), ESI-MS of **Tri-M** (C), TWIM-MS plot of **Tri-M** (D).

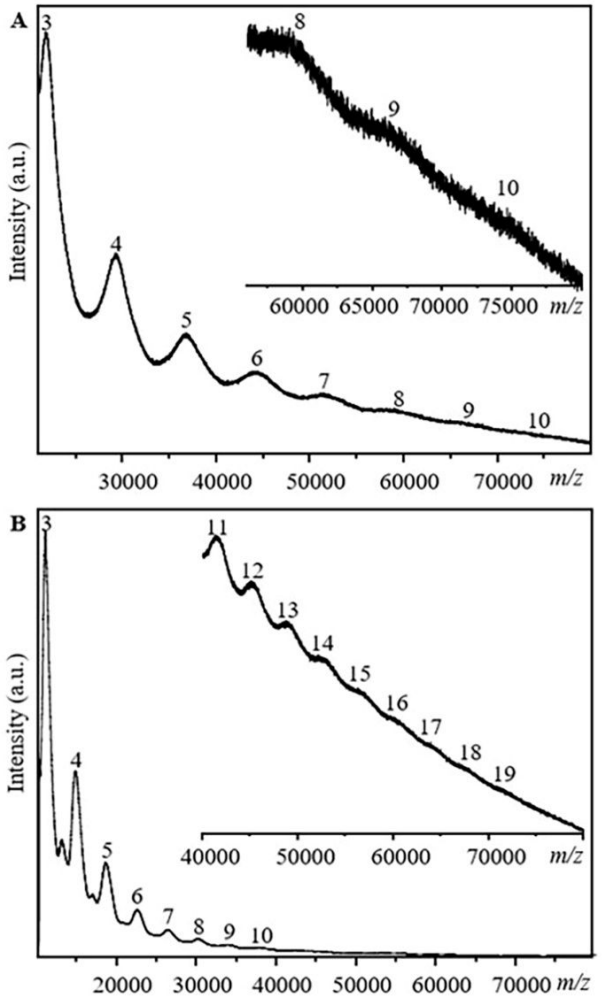

Figure 3. MALDI-TOF MS of **Hex-P** (A) and **Tri-P** (B) with corresponding numbers of repeat units in linear mode.

After polymerization, Fe(II) with weak coordination was introduced for further metalation.[25, 32, 88-93] In order to avoid the undesired crosslink between different polymer chains, low concentration (0.2 mg mL^{-1}) of metallo-polymers (**Hex-P** and **Tri-P**) was used in the metalation process. The metalation results were supported by the Ultraviolet-visible (UV-vis) absorption spectra as shown in **Figure S90**. In both metallo-polymers, the expected peak at about 496 nm was ascribed to the metal-to-ligand charge-transfer transition (MLCT) of <tpy-Ru(II)-tpy> connectivity.[21, 91, 94] After Fe(II) being introduced, a new emerging peak at about 574 nm that was attributed to the characteristic MLCT band of the <tpy-Fe(II)-tpy> was observed, indicating successful metalation.[25, 88-89, 91-94]

Furthermore, ultrahigh-vacuum, low-temperature scanning tunneling microscopy (UHV-LT-STM) was then used in an effort to characterize metallo-polymers and address the structure and conformation of polymer chains. Samples were dissolved in acetonitrile and deposited on an Ag (111) surface by drop-casting. It should be noted that in order to clearly observe a single metallo-polymer chain, low concentration (0.05 mg mL^{-1}) was used to prepare the STM sample.

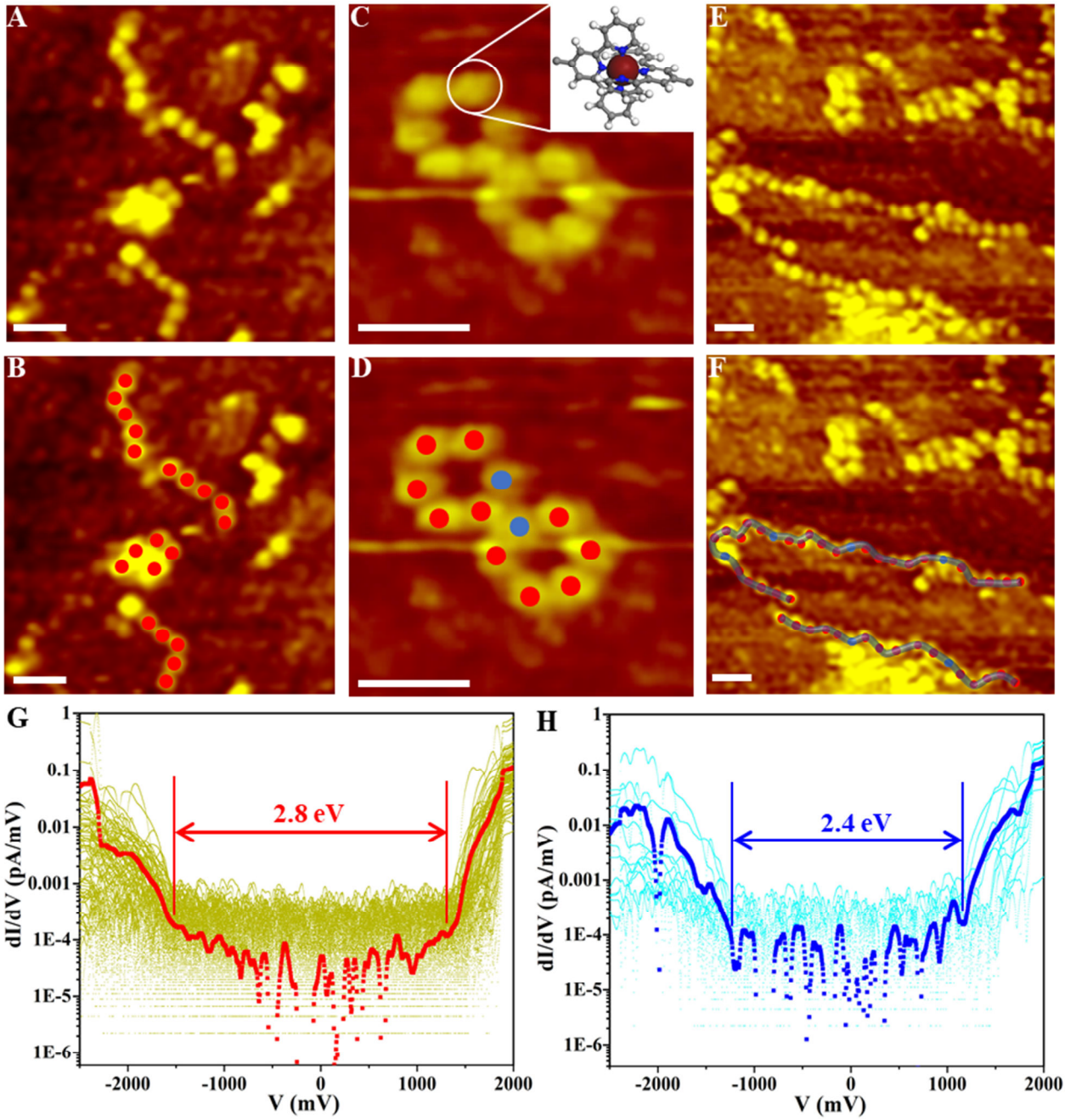

Figure 4. (A) STM image of **Hex-P** on the supporting Ag(111) surface. (B) STM image of **Hex-P** with STS data acquisition locations on <tpy-Ru(II)-tpy> unit shown in red. (C) STM image of **Hex-P-C**. (D) STS profiling of **Hex-P-C** with <tpy-Ru(II)-tpy> unit in red, and <tpy-Fe(II)-tpy> unit in blue. (E) STM image of **Hex-P-L**. (F) STS profiling of **Hex-P-L** with <tpy-Ru(II)-tpy> unit in red, and <tpy-Fe(II)-tpy> unit in blue. And the blue line in inset represents the polymer chain proposed by <tpy-metal(II)-tpy> units. dI/dV-V results of STS of (G) Ru(II) (red) and (H) Fe(II) (blue) correspond to different electronic features in (D) and (F). Scale bar: 10 nm.

Due to the octahedral coordination geometry and higher electron density around the metal ions, the <tpy-Ru(II)-tpy> or <tpy-Fe(II)-tpy> units as the stained spots gave rise to a relatively strong signal in the form of a bright lobe when compared to the organic portions.[95]

Figure 4A and **Figure S92** show the STM images of **Hex-P**, in which each of the five bright lobes located closely together correspond to five connected <tpy-Ru(II)-tpy> units, indicating the successful formation of metallo-polymers. Aggregation occurred due to the poor solubility of **Hex-P** in acetonitrile, making it difficult to observe longer polymer chains and only large bright spots are observed for aggregates as shown in **Figure S92**. We also used DMF and DMSO as solvents, which however caused severe background signals during UHV-LT-STM imaging. After self-assembly with Fe(II), six bright lobes including five <tpy-Ru(II)-tpy> units and one <tpy-Fe(II)-tpy> unit are observed as a group (**Figure 4C** and **Figure S93**). As expected, the repeat units of **Hex-P** underwent intramolecular coordination into a ring-closed structure and six bright lobes arranged in a cyclic hexagonal structure (**Hex-P-C**). The distance between two adjacent bright lobes of the cy-

clic hexagonal structure is around 2.1 nm, which is well consistent with the calculated size by modeling (**Figure S91**). Also due to the poor solubility, we were only able to observe one metallo-polymer chain with three cyclic hexagonal repeat units (**Figure S93**). Besides intramolecular coordination, intermolecular coordination into a linear chain (**Hex-P-L**) was also observed as shown in **Figure 4E** and **Figure S93**. It should originate from the constraint of the repeat units in the metallo-polymer chain, where **Alkyne-PEG** brings two monomers close enough for the occurrence of intermolecular complexation.

The positions of Fe(II) and Ru(II) ions in the repeat units were identified by the means of dI/dV-V using scanning tunneling spectroscopy (STS) that probed local density of states (LDOS).[96-97] Tunneling spectra were measured by positioning the STM tip above each lobe of the repeat units on Ag (111) surface at a fixed height with a bias range of ±2V. From dI/dV-V spectroscopic data, the energy gap between the HOMO and LUMO can be directly obtained.[98] Thus, from the STS measurements of each <tpy-metal(II)-tpy> unit, we were able to differentiate the Fe(II) and Ru(II) centers based on their different energy gaps. Among the six bright lobes of a group, one bright lobe in each group in **Figure 4C** and **4E** gives the HOMO-LUMO gap of 2.4 eV (**Figure 4H**); while the remaining five bright lobes provide the gap value of 2.8 eV (**Figure 4G**). Thus, we can identify the site with a smaller gap, *viz.* 2.4 eV, as Fe (II) and that of the larger gap, *viz.* 2.8 eV, as the Ru (II) site. Then, STM imaging was able to directly read the "sequence" of metal ion within the polymer chains (**Figure 4D** and **4F**), in which red and blue dots represent <tpy-Ru(II)-tpy> unit and <tpy-Fe(II)-tpy> unit, respectively. More importantly, the polymer chain can be profiled depending on the positions of metal ions as shown in **Figure 4F**, by which we were able to deduce the conformation of the polymer chain.

In the STM image of **Tri-P**, each of the two bright lobes positioning closely together represents two connected <tpy-Ru(II)-tpy> within a repeat unit (**Figure 5A** and **Figure S94**). With the introduction of Fe(II), all of the repeat units carried out intramolecular coordination to form a ring-closed structure, where three bright lobes arranged into a triangle (**Tri-P-C**) as evidenced by STM imaging (**Figure 5C** and **Figure S95**). And the distance between two adjacent bright lobes of the cyclic triangular structure is ca. 1.2 nm, which is well consistent with the modeling size (**Figure S91**). It should be noted that with enhanced solubility, up to 12 triangular repeat units were observed in a single polymer chain, much higher than that in the hexameric system. This result is consistent with the MALDI-TOF MS data as shown in **Figure 3**. The positions of Fe(II) and Ru(II) ions in the repeat unit are also identified by the means of dI/dV-V obtained in STS (**Figure 5E** and **5F**). We then labeled <tpy-Ru(II)-tpy> unit and <tpy-Fe(II)-tpy> unit with red and blue dots, respectively on the basis of STS results (**Figure 5B** and **5D**). The polymer chain is readily profiled using the blue dots, because all <tpy-Fe(II)-tpy> units are located right in the middle of the chain. Meanwhile, the conformation could be estimated and proposed according to the polymer chain drawn as shown in the inset of **Figure 5D**.

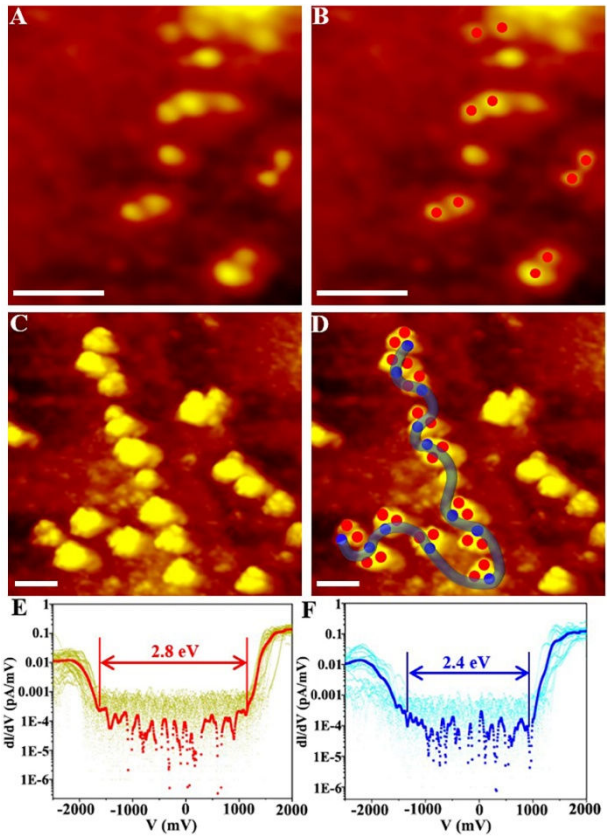

Figure 5. (A) STM image of **Tri-P** on the supporting Ag(111) surface. (B) STS profiling **Tri-P** with <tpy-Ru(II)-tpy> unit in red. (C) STM image of **Tri-P-C**. (D) STS profiling of **Tri-P-C** with <tpy-Ru(II)-tpy> unit in red, and <tpy-Fe(II)-tpy> unit in blue. And the blue line in inset represents the polymer chain proposed by <tpy-Fe(II)-tpy> units. dI/dV-V results of STS of (E) Ru(II) (red) and (F) Fe(II) (blue) correspond to different electronic features in (D). Scale bar: 5 nm.

Conclusions

In summary, a novel class of metallo-polymers were synthesized by harnessing Ru(II) with strong interaction and Fe(II) with weak interaction into one polymer system in a step-wise manner. First, open-form metal-organic monomers with Ru(II) were polymerized by click reaction to form the corresponding metallo-polymers (**Hex-P** and **Tri-P**). After further metalation by Fe(II), **Hex-P** and **Tri-P** displayed different coordination or self-assembly behaviors. More importantly, the structures and conformations of single polymer chains can be directly visualized through STM and STS of the <tpy-metal(II)-tpy> units. The metallo-polymers generated by **Hex-P** include not only hexagons constructed by intramolecular coordination, but also hexameric linear chains formed by intermolecular coordination. In a sharp contrast, the further coordination of **Tri-P** was carried out in a more controlled manner with only intramolecular complexation observed to form triangles as the repeat units. The different results are attributed to the size and rigidity of the repeat units. Overall, our endeavors will bring innovative aspects into polymer chemistry field and shed light on the development of innovative approaches to synthesize metallo-polymers and study the structure and conformation of polymer chains at single-molecule level. The characterization with the combination

of STM and STS could be expanded into other metallo-polymer systems to advance our understanding of the structure-property relationship of polymers.

ASSOCIATED CONTENT

Supporting Information. Instrumentations, synthetic details, molecular modeling, monomer and polymer characterization, including ^{1}H NMR, ^{13}C NMR, 2D COSY, 2D NOESY, ESI-MS, UV-vis and additional STM images are included in supporting information. This material is available free of charge via the Internet at http://pubs.acs.org.

AUTHOR INFORMATION

Corresponding Author

*shla@anl.gov
*tuyingfeng@suda.edu.cn
*xiaopengli1@usf.edu

Author Contributions

⊥These authors contributed equally.

Notes

The authors declare no competing financial interest.

ACKNOWLEDGMENT

We acknowledge the support from National Institutes of Health (R01GM128037) and National Science Foundation of China (21774090). Use of the Center for Nanoscale Materials, an Office of Science user facility, was supported by the U.S. Department of Energy, Office of Science, Office of Basic Energy Sciences, under Contract No. DE-AC02-06CH11357. We also acknowledge partial support through University of South Florida Nexus Initiative (UNI) Award, and the Priority Academic Program Development of Jiangsu Higher Education Institutions (PAPD).

REFERENCES

1. Kumaki, J.; Sakurai, S.-i.; Yashima, E. Visualization of Synthetic Helical Polymers by High-Resolution Atomic Force Microscopy. *Chem. Soc. Rev.* **2009,** *38*, 737-746.
2. Ouchi, M.; Badi, N.; Lutz, J.-F.; Sawamoto, M. Single-Chain Technology Using Discrete Synthetic Macromolecules. *Nat. Chem.* **2011,** *3*, 917-924.
3. Hansma, H. G.; Vesenka, J.; Siegerist, C.; Kelderman, G.; Morrett, H.; Sinsheimer, R. L.; Elings, V.; Bustamante, C.; Hansma, P. K. Reproducible Imaging and Dissection of Plasmid DNA Under Liquid with the Atomic Force Microscope. *Science* **1992,** *256*, 1180-1184.
4. Guckenberger, R.; Heim, M.; Cevc, G.; Knapp, H.; Wiegräbe, W.; Hillebrand, A. Scanning Tunneling Microscopy of Insulators and Biological Specimens Based on Lateral Conductivity of Ultrathin Water Films. *Science* **1994,** *266*, 1538-1540.
5. Adamcik, J.; Klinov, D. V.; Witz, G.; Sekatskii, S. K.; Dietler, G. Observation of Single-Stranded DNA on Mica and Highly Oriented Pyrolytic Graphite by Atomic Force Microscopy. *FEBS Lett.* **2006,** *580*, 5671-5675.
6. Leung, C.; Bestembayeva, A.; Thorogate, R.; Stinson, J.; Pyne, A.; Marcovich, C.; Yang, J.; Drechsler, U.; Despont, M.; Jankowski, T.; Tschöpe, M.; Hoogenboom, B. W. Atomic Force Microscopy with Nanoscale Cantilevers Resolves Different Structural Conformations of the DNA Double Helix. *Nano Lett.* **2012,** *12*, 3846-3850.
7. Terasaki, K.; Yokoyama, T. Structural Modification of DNA Studied by Scanning Tunneling Microscopy. *J. Phys. Chem. B* **2019,** *123*, 1780-1783.
8. Abe, H.; Kikkawa, Y.; Iwata, T.; Aoki, H.; Akehata, T.; Doi, Y. Microscopic Visualization on Crystalline Morphologies of Thin Films for Poly[(R)-3-hydroxybutyric acid] and Its Copolymer. *Polymer* **2000,** *41*, 867-874.
9. Reiter, G.; Castelein, G.; Sommer, J.-U.; Röttele, A.; Thurn-Albrecht, T. Direct Visualization of Random Crystallization and Melting in Arrays of Nanometer-Size Polymer Crystals. *Phys. Rev. Lett.* **2001,** *87*, 226101.
10. Banno, M.; Wu, Z.-Q.; Nagai, K.; Sakurai, S.-i.; Okoshi, K.; Yashima, E. Two-Dimensional Bilayer Smectic Ordering of Rigid Rod-Rod Helical Diblock Polyisocyanides. *Macromolecules* **2010,** *43*, 6553-6561.
11. Kumaki, J.; Nishikawa, Y.; Hashimoto, T. Visualization of Single-Chain Conformations of a Synthetic Polymer with Atomic Force Microscopy. *J. Am. Chem. Soc.* **1996,** *118*, 3321-3322.
12. Sakaguchi, H.; Matsumura, H.; Gong, H.; Abouelwafa, A. M. Direct Visualization of the Formation of Single-Molecule Conjugated Copolymers. *Science* **2005,** *310*, 1002-1006.
13. Kumaki, J.; Kajitani, T.; Nagai, K.; Okoshi, K.; Yashima, E. Visualization of Polymer Chain Conformations in Amorphous Polyisocyanide Langmuir-Blodgett Films by Atomic Force Microscopy. *J. Am. Chem. Soc.* **2010,** *132*, 5604-5606.
14. Banno, M.; Yamaguchi, T.; Nagai, K.; Kaiser, C.; Hecht, S.; Yashima, E. Optically Active, Amphiphilic Poly(meta-phenylene ethynylene)s: Synthesis, Hydrogen-Bonding Enforced Helix Stability, and Direct AFM Observation of Their Helical Structures. *J. Am. Chem. Soc.* **2012,** *134*, 8718-8728.
15. Guan, W.; Wang, G.; Ding, J.; Li, B.; Wu, L. A Supramolecular Approach of Modified Polyoxometalate Polymerization and Visualization of a Single Polymer Chain. *Chem. Commun.* **2019,** *55*, 10788-10791.
16. Hailes, R. L. N.; Oliver, A. M.; Gwyther, J.; Whittell, G. R.; Manners, I. Polyferrocenylsilanes: Synthesis, Properties, and Applications. *Chem. Soc. Rev.* **2016,** *45*, 5358-5407.
17. Yan, Y.; Zhang, J.; Ren, L.; Tang, C. Metal-Containing and Related Polymers for Biomedical Applications. *Chem. Soc. Rev.* **2016,** *45*, 5232-5263.
18. Zha, Y.; Disabb-Miller, M. L.; Johnson, Z. D.; Hickner, M. A.; Tew, G. N. Metal-Cation-Based Anion Exchange Membranes. *J. Am. Chem. Soc.* **2012,** *134*, 4493-4496.
19. Yan, X.; Li, S.; Pollock, J. B.; Cook, T. R.; Chen, J.; Zhang, Y.; Ji, X.; Yu, Y.; Huang, F.; Stang, P. J. Supramolecular Polymers with Tunable Topologies via Hierarchical Coordination-Driven Self-Assembly and Hydrogen Bonding Interfaces. *Proc. Natl. Acad. Sci. U.S.A.* **2013,** *110*, 15585-15590.
20. Zhang, M.; Li, S.; Yan, X.; Zhou, Z.; Saha, M. L.; Wang, Y.-C.; Stang, P. J. Fluorescent Metallacycle-Cored Polymers via Covalent Linkage and Their Use as Contrast Agents for Cell Imaging. *Proc. Natl. Acad. Sci. U.S.A.* **2016,** *113*, 11100-11105.
21. Kelch, S.; Rehahn, M. Synthesis and Properties in Solution of Rodlike, 2,2′:6′,2″-Terpyridine-Based Ruthenium(II) Coordination Polymers. *Macromolecules* **1999,** *32*, 5818-5828.
22. Beck, J. B.; Rowan, S. J. Multistimuli, Multiresponsive Metallo-Supramolecular Polymers. *J. Am. Chem. Soc.* **2003,** *125*, 13922-13923.
23. Dobrawa, R.; Würthner, F. Metallosupramolecular Approach toward Functional Coordination Polymers. *J. Polym. Sci., Part A: Polym. Chem.* **2005,** *43*, 4981-4995.
24. Hofmeier, H.; Hoogenboom, R.; Wouters, M. E. L.; Schubert, U. S. High Molecular Weight Supramolecular Polymers Containing Both Terpyridine Metal Complexes and Ureidopyrimidinone Quadruple Hydrogen-Bonding Units in the Main Chain. *J. Am. Chem. Soc.* **2005,** *127*, 2913-2921.
25. Han, F. S.; Higuchi, M.; Kurth, D. G. Metallo-Supramolecular Polymers Based on Functionalized Bis-

terpyridines as Novel Electrochromic Materials. *Adv. Mater.* **2007,** *19*, 3928-3931.

26. Winter, A.; Friebe, C.; Chiper, M.; Hager, M. D.; Schubert, U. S. Self-Assembly of π-Conjugated Bis(terpyridine) Ligands with Zinc(II) Ions: New Metallosupramolecular Materials for Optoelectronic Applications. *J. Polym. Sci., Part A: Polym. Chem.* **2009,** *47*, 4083-4098.

27. Burnworth, M.; Tang, L.; Kumpfer, J. R.; Duncan, A. J.; Beyer, F. L.; Fiore, G. L.; Rowan, S. J.; Weder, C. Optically Healable Supramolecular Polymers. *Nature* **2011,** *472*, 334-337.

28. Padhy, H.; Sahu, D.; Chiang, I-H.; Patra, D.; Kekuda, D.; Chu, C.-W.; Lin, H.-C. Synthesis and Applications of Main-Chain Ru(II) Metallo-Polymers Containing Bis-Terpyridyl Ligands with Various Benzodiazole Cores for Solar Cells. *J. Mater. Chem.* **2011,** *21*, 1196-1205.

29. Miller, A. K.; Li, Z.; Streletzky, K. A.; Jamieson, A. M.; Rowan, S. J. Redox-Induced Polymerisation/Depolymerisation of Metallo-Supramolecular Polymers. *Polym. Chem.* **2012,** *3*, 3132-3138.

30. Borré, E.; Stumbé, J.-F.; Bellemin-Laponnaz, S.; Mauro, M. Light-Powered Self-Healable Metallosupramolecular Soft Actuators. *Angew. Chem. Int. Ed.* **2016,** *55*, 1313-1317.

31. Yan, X.; Xu, J.-F.; Cook, T. R.; Huang, F.; Yang, Q.-Z.; Tung, C.-H.; Stang, P. J. Photoinduced Transformations of Stiff-Stilbene-Based Discrete Metallacycles to Metallosupramolecular Polymers. *Proc. Natl. Acad. Sci. U.S.A.* **2014,** *111*, 8717-8722.

32. Bode, S.; Zedler, L.; Schacher, F. H.; Dietzek, B.; Schmitt, M.; Popp, J.; Hager, M. D.; Schubert, U. S. Self-Healing Polymer Coatings Based on Crosslinked Metallosupramolecular Copolymers. *Adv. Mater.* **2013,** *25*, 1634-1638.

33. Michal, B. T.; McKenzie, B. M.; Felder, S. E.; Rowan, S. J. Metallo-, Thermo-, and Photoresponsive Shape Memory and Actuating Liquid Crystalline Elastomers. *Macromolecules* **2015,** *48*, 3239-3246.

34. Li, C.-H.; Wang, C.; Keplinger, C.; Zuo, J.-L.; Jin, L.; Sun, Y.; Zheng, P.; Cao, Y.; Lissel, F.; Linder, C.; You, X.-Z.; Bao, Z. A Highly Stretchable Autonomous Self-Healing Elastomer. *Nat. Chem.* **2016,** *8*, 618-624.

35. Tang, Z.; Huang, J.; Guo, B.; Zhang, L.; Liu, F. Bioinspired Engineering of Sacrificial Metal-Ligand Bonds into Elastomers with Supramechanical Performance and Adaptive Recovery. *Macromolecules* **2016,** *49*, 1781-1789.

36. Zhang, X.; Tang, Z.; Guo, B.; Zhang, L. Enabling Design of Advanced Elastomer with Bioinspired Metal-Oxygen Coordination. *ACS Appl. Mater. Interfaces* **2016,** *8*, 32520-32527.

37. Filippidi, E.; Cristiani, T. R.; Eisenbach, C. D.; Waite, J. H.; Israelachvili, J. N.; Ahn, B. K.; Valentine, M. T. Toughening Elastomers Using Mussel-Inspired Iron-Catechol Complexes. *Science* **2017,** *358*, 502-505.

38. Yang, L.; Zhang, G.; Zheng, N.; Zhao, Q.; Xie, T. A Metallosupramolecular Shape-Memory Polymer with Gradient Thermal Plasticity. *Angew. Chem. Int. Ed.* **2017,** *56*, 12599-12602.

39. Whittell, G. R.; Hager, M. D.; Schubert, U. S.; Manners, I. Functional Soft Materials from Metallopolymers and Metallosupramolecular Polymers. *Nat. Mater.* **2011,** *10*, 176-188.

40. Weng, G.; Thanneeru, S.; He, J. Dynamic Coordination of Eu-Iminodiacetate to Control Fluorochromic Response of Polymer Hydrogels to Multistimuli. *Adv. Mater.* **2018,** *30*, 1706526.

41. Thanneeru, S.; Milazzo, N.; Lopes, A.; Wei, Z.; Angeles-Boza, A. M.; He, J. Synthetic Polymers To Promote Cooperative Cu Activity for O_2 Activation: Poly vs Mono. *J. Am. Chem. Soc.* **2019,** *141*, 4252-4256.

42. Zhou, X.; Wang, L.; Wei, Z.; Weng, G.; He, J. An Adaptable Tough Elastomer with Moisture-Triggered Switchable Mechanical and Fluorescent Properties. *Adv. Funct. Mater.* **2019,** *29*, 1903543.

43. Aamer, K. A.; Tew, G. N. Supramolecular Polymers Containing Terpyridine-Metal Complexes in the Side Chain. *Macromolecules* **2007,** *40*, 2737-2744.

44. Gu, H.; Ciganda, R.; Gatard, S.; Lu, F.; Zhao, P.; Ruiz, J.; Astruc, D. On Metallocene-Containing Macromolecules and Their Applications. *J. Organomet. Chem.* **2016,** *813*, 95-102.

45. Yang, P.; Pageni, P.; Kabir, M. P.; Zhu, T.; Tang, C. Metallocene-Containing Homopolymers and Heterobimetallic Block Copolymers via Photoinduced RAFT Polymerization. *ACS Macro Lett.* **2016,** *5*, 1293-1300.

46. Sha, Y.; Zhang, Y.; Zhu, T.; Tan, S.; Cha, Y.; Craig, S. L.; Tang, C. Ring-Closing Metathesis and Ring-Opening Metathesis Polymerization toward Main-Chain Ferrocene-Containing Polymers. *Macromolecules* **2018,** *51*, 9131-9139.

47. Gu, Y.; Alt, E. A.; Wang, H.; Li, X.; Willard, A. P.; Johnson, J. A. Photoswitching Topology in Polymer Networks with Metal–Organic Cages as Crosslinks. *Nature* **2018,** *560*, 65-69.

48. Lehn, J.-M. From Supramolecular Chemistry towards Constitutional Dynamic Chemistry and Adaptive Chemistry. *Chem. Soc. Rev.* **2007,** *36*, 151-160.

49. Forgan, R. S.; Sauvage, J.-P.; Stoddart, J. F. Chemical Topology: Complex Molecular Knots, Links, and Entanglements. *Chem. Rev.* **2011,** *111*, 5434-5464.

50. Chakrabarty, R.; Mukherjee, P. S.; Stang, P. J. Supramolecular Coordination: Self-Assembly of Finite Two- and Three-Dimensional Ensembles. *Chem. Rev.* **2011,** *111*, 6810-6918.

51. Cook, T. R.; Stang, P. J. Recent Developments in the Preparation and Chemistry of Metallacycles and Metallacages via Coordination. *Chem. Rev.* **2015,** *115*, 7001-7045.

52. Yoshizawa, M.; Klosterman, J. K.; Fujita, M. Functional Molecular Flasks: New Properties and Reactions within Discrete, Self-Assembled Hosts. *Angew. Chem. Int. Ed.* **2009,** *48*, 3418-3438.

53. Harris, K.; Fujita, D.; Fujita, M. Giant Hollow M_nL_{2n} Spherical Complexes: Structure, Functionalisation and Applications. *Chem. Commun.* **2013,** *49*, 6703-6712.

54. McConnell, A. J.; Wood, C. S.; Neelakandan, P. P.; Nitschke, J. R. Stimuli-Responsive Metal-Ligand Assemblies. *Chem. Rev.* **2015,** *115*, 7729-7793.

55. Zarra, S.; Wood, D. M.; Roberts, D. A.; Nitschke, J. R. Molecular Containers in Complex Chemical Systems. *Chem. Soc. Rev.* **2015,** *44*, 419-432.

56. Ayme, J.-F.; Beves, J. E.; Campbell, C. J.; Leigh, D. A. Template Synthesis of Molecular Knots. *Chem. Soc. Rev.* **2013,** *42*, 1700-1712.

57. Chakraborty, S.; Newkome, G. R. Terpyridine-Based Metallosupramolecular Constructs: Tailored Monomers to Precise 2D-Motifs and 3D-Metallocages. *Chem. Soc. Rev.* **2018,** *47*, 3991-4016.

58. Han, M.; Engelhard, D. M.; Clever, G. H. Self-Assembled Coordination Cages Based on Banana-Shaped Ligands. *Chem. Soc. Rev.* **2014,** *43*, 1848-1860.

59. De, S.; Mahata, K.; Schmittel, M. Metal-Coordination-Driven Dynamic Heteroleptic Architectures. *Chem. Soc. Rev.* **2010,** *39*, 1555-1575.

60. Saha, M. L.; De, S.; Pramanik, S.; Schmittel, M. Orthogonality in Discrete Self-Assembly - Survey of Current Concepts. *Chem. Soc. Rev.* **2013,** *42*, 6860-6909.

61. Qi, Z.; Heinrich, T.; Moorthy, S.; Schalley, C. A. Gas-Phase Chemistry of Molecular Containers. *Chem. Soc. Rev.* **2015,** *44*, 515-531.

62. Würthner, F.; You, C.-C.; Saha-Möller, C. R. Metallosupramolecular Squares: from Structure to Function. *Chem. Soc. Rev.* **2004,** *33*, 133-146.

63. Chen, L.-J.; Yang, H.-B.; Shionoya, M. Chiral Metallosupramolecular Architectures. *Chem. Soc. Rev.* **2017,** *46*, 2555-2576.

64. Jin, P.; Dalgarno, S. J.; Atwood, J. L. Mixed Metal-Organic Nanocapsules. *Coord. Chem. Rev.* **2010,** *254*, 1760-1768.

65. Leininger, S.; Olenyuk, B.; Stang, P. J. Self-Assembly of Discrete Cyclic Nanostructures Mediated by Transition Metals. *Chem. Rev.* **2000,** *100*, 853-908.

66. Olenyuk, B.; Whiteford, J. A.; Fechtenkötter, A.; Stang, P. J. Self-Assembly of Nanoscale Cuboctahedra by Coordination Chemistry. *Nature* **1999,** *398*, 796-799.

67. Sun, Q.-F.; Iwasa, J.; Ogawa, D.; Ishido, Y.; Sato, S.; Ozeki, T.; Sei, Y.; Yamaguchi, K.; Fujita, M. Self-Assembled $M_{24}L_{48}$ Polyhedra and Their Sharp Structural Switch Upon Subtle Ligand Variation. *Science* **2010,** *328*, 1144-1147.

68. Fujita, D.; Ueda, Y.; Sato, S.; Mizuno, N.; Kumasaka, T.; Fujita, M. Self-Assembly of Tetravalent Goldberg Polyhedra from 144 Small Components. *Nature* **2016,** *540*, 563-566.

69. Cook, T. R.; Zheng, Y.-R.; Stang, P. J. Metal-Organic Frameworks and Self-Assembled Supramolecular Coordination Complexes: Comparing and Contrasting the Design, Synthesis, and Functionality of Metal-Organic Materials. *Chem. Rev.* **2013,** *113*, 734-777.

70. Sun, Y.; Chen, C.; Stang, P. J. Soft Materials with Diverse Suprastructures via the Self-Assembly of Metal-Organic Complexes. *Acc. Chem. Res.* **2019,** *52*, 802-817.

71. Stang, P. J.; Olenyuk, B. Self-Assembly, Symmetry, and Molecular Architecture: Coordination as the Motif in the Rational Design of Supramolecular Metallacyclic Polygons and Polyhedra. *Acc. Chem. Res.* **1997,** *30*, 502-518.

72. Wang, W.; Wang, Y.-X.; Yang, H.-B. Supramolecular Transformations within Discrete Coordination-Driven Supramolecular Architectures. *Chem. Soc. Rev.* **2016,** *45*, 2656-2693.

73. Hein, J. E.; Fokin, V. V. Copper-Catalyzed Azide-Alkyne Cycloaddition (CuAAC) and Beyond: New Reactivity of Copper(I) Acetylides. *Chem. Soc. Rev.* **2010,** *39*, 1302-1315.

74. Liang, L.; Astruc, D. The Copper(I)-Catalyzed Alkyne-Azide Cycloaddition (CuAAC) "Click" Reaction and Its Applications. An Overview. *Coord. Chem. Rev.* **2011,** *255*, 2933-2945.

75. Li, Y.; Zhou, C.; Xu, L.; Yao, F.; Cen, L.; Fu, G. D. Stimuli-Responsive Hydrogels Prepared by Simultaneous "Click Chemistry" and Metal-Ligand Coordination. *RSC Adv.* **2015,** *5*, 18242-18251.

76. Singh, M. S.; Chowdhury, S.; Koley, S. Advances of Azide-Alkyne Cycloaddition-Click Chemistry over the Recent Decade. *Tetrahedron* **2016,** *72*, 5257-5283.

77. Newkome, G. R.; Wang, P.; Moorefield, C. N.; Cho, T. J.; Mohapatra, P. P.; Li, S.; Hwang, S.-H.; Lukoyanova, O.; Echegoyen, L.; Palagallo, J. A.; Iancu, V.; Hla, S.-W. Nanoassembly of a Fractal Polymer: A Molecular "Sierpinski Hexagonal Gasket". *Science* **2006,** *312*, 1782-1785.

78. Granzhan, A.; Schouwey, C.; Riis-Johannessen, T.; Scopelliti, R.; Severin, K. Connection of Metallamacrocycles via Dynamic Covalent Chemistry: A Versatile Method for the Synthesis of Molecular Cages. *J. Am. Chem. Soc.* **2011,** *133*, 7106-7115.

79. Li, K.; Zhang, L.-Y.; Yan, C.; Wei, S.-C.; Pan, M.; Zhang, L.; Su, C.-Y. Stepwise Assembly of $Pd_6(RuL_3)_8$ Nanoscale Rhombododecahedral Metal-Organic Cages via Metalloligand Strategy for Guest Trapping and Protection. *J. Am. Chem. Soc.* **2014,** *136*, 4456-4459.

80. Lu, X.; Li, X.; Guo, K.; Xie, T.-Z.; Moorefield, C. N.; Wesdemiotis, C.; Newkome, G. R. Probing a Hidden World of Molecular Self-Assembly: Concentration-Dependent, Three-Dimensional Supramolecular Interconversions. *J. Am. Chem. Soc.* **2014,** *136*, 18149-18155.

81. Newkome, G. R.; Moorefield, C. N. From 1 → 3 Dendritic Designs to Fractal Supramacromolecular Constructs: Understanding the Pathway to the Sierpiński Gasket. *Chem. Soc. Rev.* **2015,** *44*, 3954-3967.

82. Li, Y.; Jiang, Z.; Wang, M.; Yuan, J.; Liu, D.; Yang, X.; Chen, M.; Yan, J.; Li, X.; Wang, P. Giant, Hollow 2D Metalloarchitecture: Stepwise Self-Assembly of a Hexagonal Supramolecular Nut. *J. Am. Chem. Soc.* **2016,** *138*, 10041-10046.

83. Jiang, Z.; Li, Y.; Wang, M.; Liu, D.; Yuan, J.; Chen, M.; Wang, J.; Newkome, G. R.; Sun, W.; Li, X.; Wang, P. Constructing High-Generation Sierpiński Triangles by Molecular Puzzling. *Angew. Chem. Int. Ed.* **2017,** *56*, 11450-11455.

84. Zhang, Z.; Wang, H.; Wang, X.; Li, Y.; Song, B.; Bolarinwa, O.; Reese, R. A.; Zhang, T.; Wang, X.-Q.; Cai, J.; Xu, B.; Wang, M.; Liu, C.; Yang, H.-B.; Li, X. Supersnowflakes: Stepwise Self-Assembly and Dynamic Exchange of Rhombus Star-Shaped Supramolecules. *J. Am. Chem. Soc.* **2017,** *139*, 8174-8185.

85. Schmatloch, S.; van den Berg, A. M. J.; Alexeev, A. S.; Hofmeier, H.; Schubert, U. S. Soluble High-Molecular-Mass Poly(ethylene oxide)s via Self-Organization. *Macromolecules* **2003,** *36*, 9943-9949.

86. Montaudo, G.; Samperi, F.; Montaudo, M. S. Characterization of Synthetic Polymers by MALDI-MS. *Prog. Polym. Sci.* **2006,** *31*, 277-357.

87. Li, Z.; Gu, J.; Qi, S.; Wu, D.; Gao, L.; Chen, Z.; Guo, J.; Li, X.; Wang, Y.; Yang, X.; Tu, Y. Shackling Effect Induced Property Differences in Metallo-Supramolecular Polymers. *J. Am. Chem. Soc.* **2017,** *139*, 14364-14367.

88. Hofmeier, H.; Schubert, U. S. Supramolecular Branching and Crosslinking of Terpyridine-Modified Copolymers: Complexation and Decomplexation Studies in Diluted Solution. *Macromol. Chem. Phys.* **2003,** *204*, 1391-1397.

89. Beck, J. B.; Ineman, J. M.; Rowan, S. J. Metal/Ligand-Induced Formation of Metallo-Supramolecular Polymers. *Macromolecules* **2005,** *38*, 5060-5068.

90. Knapton, D.; Rowan, S. J.; Weder, C. Synthesis and Properties of Metallo-Supramolecular Poly(p-phenylene ethynylene)s. *Macromolecules* **2006,** *39*, 651-657.

91. Hu, C.-W.; Sato, T.; Zhang, J.; Moriyama, S.; Higuchi, M. Multi-Colour Electrochromic Properties of Fe/Ru-Based Bimetallo-Supramolecular Polymers. *J. Mater. Chem. C* **2013,** *1*, 3408-3413.

92. Gao, L.; Zhang, Z.; Zheng, B.; Huang, F. Construction of Muscle-Like Metallo-Supramolecular Polymers from a Pillar[5]Arene-Based [*c*2]Daisy Chain. *Polym. Chem.* **2014,** *5*, 5734-5739.

93. Hu, C.-W.; Sato, T.; Zhang, J.; Moriyama, S.; Higuchi, M. Three-Dimensional Fe(II)-based Metallo-Supramolecular Polymers with Electrochromic Properties of Quick Switching, Large Contrast, and High Coloration Efficiency. *ACS Appl. Mater. Interfaces* **2014,** *6*, 9118-9125.

94. Li, Y.; Jiang, Z.; Yuan, J.; Liu, D.; Wu, T.; Moorefield, C. N.; Newkome, G. R.; Wang, P. Facile Thermodynamic Conversion of a Linear Metallopolymer into a Self-Assembled Hexameric Metallomacrocycle. *Chem. Commun.* **2015,** *51*, 5766-5769.

95. Wang, H.; Li, Y.; Yu, H.; Song, B.; Lu, S.; Hao, X.-Q.; Zhang, Y.; Wang, M.; Hla, S.-W.; Li, X. Combining Synthesis and Self-Assembly in One Pot To Construct Complex 2D Metallo-Supramolecules Using Terpyridine and Pyrylium Salts. *J. Am. Chem. Soc.* **2019,** *141*, 13187-13195.

96. Hasegawa, Y.; Avouris, P. Hasegawa, Y. & Avouris, P. Direct Observation of Standing Wave Formation at Surface Steps Using STS. *Phys. Rev. Lett.* **1993,** *71*, 1071-1074.

97. Yan, C.; Ma, D.-L.; Qiao, J.-B.; Zhong, H.-Y.; Yang, L.; Li, S.-Y.; Fu, Z.-Q.; Zhang, Y.; He, L. Scanning Tunneling Microscopy Study of the Quasicrystalline 30° Twisted Bilayer Graphene. *2D Materials* **2019,** *6*, 045041.

98. Hess, H. F.; Robinson, R. B.; Dynes, R. C.; Valles, J. M.; Waszczak, J. V. Scanning-Tunneling-Microscope Observation of the Abrikosov Flux Lattice and the Density of States near and inside a Fluxoid. *Phys. Rev. Lett.* **1989,** *62*, 214-216.

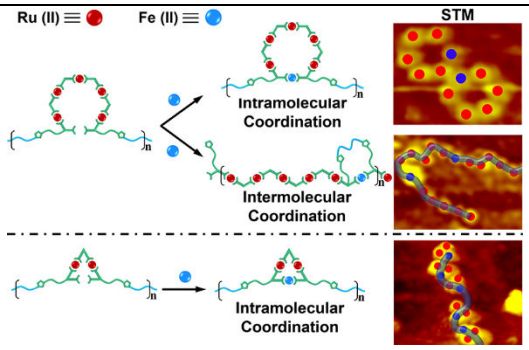

Insert Table of Contents